WEP Warwick Evans Publishing

Transactions on Engineering and Technology Research
ISSN: 2960-1797, eISSN: 2960-2246 | Volume 6
MECEME 2026

A Simulation Study on Object Motion under Air Resistance Based on Python Modeling

Yuyang Qi *, Jingbin Xue, Dechao Lv

School of physics, Hangzhou Normal University, HangZhou, China

* Corresponding Author Email: 2025112030015@stu.hznu.edu.cn

Abstract. This article focuses on the influence of air resistance on object motion, and constructs and compares four models: constant resistance, linear resistance, quadratic resistance, and polynomial resistance. The analytical forms of velocity and displacement were derived at the theoretical level, and the evolution of motion over time was visually presented through Python numerical simulation. The results indicate that different forms of resistance determine the existence and magnitude of the ultimate speed, as well as the speed at which motion tends to steady state. The study not only revealed the differences between ideal models and actual motion, but also demonstrated the value of numerical simulation in physics teaching and research.

Keywords: Air resistance; maximum speed; Resistance model; numerical simulation.

1. Introduction

In the primary research of classical mechanics, the influence of air resistance is usually ignored when analyzing the motion state of objects. This simplification can make the problem easier to analyze, but there is a significant deviation from the real environment. For example, research has shown that raindrops do not accelerate infinitely during their descent, but rather approach a finite terminal velocity [1]; Badminton rapidly decelerates during flight, which is significantly different from the parabolic trajectory of an ideal projectile [2][3]; For example, when a spacecraft re-enters the atmosphere, air resistance not only causes rapid velocity decay, but also relates to heat accumulation and safe return [4]. These phenomena indicate that studying the influence of air resistance on object motion not only has theoretical significance, but also has important practical value.

There are three common modeling methods for air resistance. One is approximately constant resistance, commonly used in low-speed or simplified scenarios [5]; The second is linear resistance proportional to velocity, which is suitable for low-speed situations dominated by viscous flow [6]; The third is the quadratic resistance proportional to the square of the velocity, which is common in high-speed situations dominated by turbulence [7]. In more complex environments, resistance can even be expressed in polynomial form of velocity to simultaneously consider the superposition of different physical effects [8]. Comparing and analyzing different resistance models not only helps to reveal the diversity of object motion laws, but also helps learners better understand the differences between ideal models and actual motion [9]. Meanwhile, by combining numerical simulation methods, the evolution process of velocity and displacement over time can be visually presented, thus playing an important role in teaching and research [10]. Based on this, this article intends to construct different models for constant resistance, linear resistance, quadratic resistance, and polynomial resistance, analyze them from both theoretical derivation and numerical simulation, and provide corresponding velocity-time and displacement-time curves.

2. Theoretical Models

2.1. Basic Equations of Motion

When an object falls in a gravitational field, its dynamic laws can be given by Newton's second law:

$$m\frac{dv}{dt} = mg - F_d \tag{1}$$

Among them, m is the mass of the object, g is the acceleration due to gravity, v is the velocity (specified as positive downwards), and F_d represents air resistance. To simplify the analysis, this article assumes that the object is released from rest, with an initial velocity of $v(0) = 0$, and begins to fall from the reference position $y(0) = 0$. Therefore, in subsequent derivations, the expressions for velocity and displacement are based on this initial condition. The specific form of air resistance depends on the velocity range of the object's motion and fluid dynamics effects, and several common models are as follows.

2.2. Constant Resistance Model

Assuming the air resistance is a constant F_0, substituting it into equation (1) yields:

$$m\frac{dv}{dt} = mg - F_0 \tag{2}$$

At this moment, the acceleration is:

$$a = g - \frac{F_0}{m} \tag{3}$$

If $mg = F_0$, the object will remain stationary without initial velocity.

If $mg > F_0$ and acceleration remain positive, the object will continue to accelerate:

$$v(t) = (g - \frac{F_0}{m})t \tag{4}$$

By integrating equation (4), the variation law of object displacement with time can be obtained:

$$y(t) = \frac{1}{2}(g - \frac{F_0}{m})t^2 \tag{5}$$

At this point, the motion of the object is similar to free fall, but the "equivalent acceleration" decreases to $g - \frac{F_0}{m}$. This means that the object will not reach its maximum velocity during the falling process, and its velocity will increase infinitely.

2.3. Linear Resistance Model

Assuming that air resistance is proportional to velocity, i.e. $F_d = kv$, substitute into equation (1) to obtain:

$$m\frac{dv}{dt} = mg - kv \tag{6}$$

Sort out the first-order linear differential equation:

$$\int \frac{dv}{g - \frac{k}{m}v} = \int dt \tag{7}$$

Understood:

$$v(t) = \frac{mg}{k}(1 - e^{-\frac{k}{m}t}) \tag{8}$$

By integrating equation (8), the variation law of object displacement with time can be obtained:

$$y(t) = \frac{mg}{k}[t + \frac{m}{k}(e^{-\frac{k}{m}t} - 1)] \tag{9}$$

According to equation (8), the velocity of an object in the linear resistance model does not increase infinitely, but gradually approaches the ultimate velocity $v_\infty = \frac{mg}{k}$ in an exponential form. This is because the resistance increases linearly with velocity, and when it is in equilibrium with gravity, the net force is zero, resulting in a uniform falling state. The time constant $\tau = \frac{m}{k}$ in the exponential term describes the convergence rate. At a time of approximately τ, the speed has reached 63% of the maximum speed, and is almost approaching steady state at around 3τ. From equation (9), it can be further observed that the exponential term has not yet decayed during the initial stage of motion, and the displacement is approximately parabolic. As time passes, the exponential term gradually disappears, and the displacement curve gradually transforms from a parabolic curve to a straight line with a slope of v_∞.

2.4. Secondary Resistance Model

Assuming that air resistance is proportional to the square of velocity, i.e. $F F_d = cv^2$, substitute into equation (1) to obtain:

$$m\frac{dv}{dt} = mg - cv^2 \tag{10}$$

Organized nonlinear differential equations:

$$\int \frac{dv}{g - \frac{c}{m}v^2} = \int dt \tag{11}$$

Understood:

$$v(t) = \sqrt{\frac{mg}{c}}\tanh(\sqrt{\frac{gc}{m}}t) \tag{12}$$

By integrating equation (12), the variation law of object displacement with time can be obtained:

$$y(t) = \frac{m}{c}\ln\cosh(\sqrt{\frac{gc}{m}}t) \tag{13}$$

According to equation (12), the velocity of an object under the quadratic resistance model increases in the form of a hyperbolic tangent function over time and rapidly approaches the ultimate velocity $v_\infty = \sqrt{\frac{mg}{c}}$ within a finite time scale. Compared with linear resistance, the resistance in this model increases faster with velocity, so the object reaches equilibrium earlier. Specifically, as the speed gradually approaches v_∞, the acceleration rapidly decays and the motion quickly enters a stable, uniform descent phase. From equation (13), it can be seen that the displacement curve during the initial stage of motion is still close to the quadratic function of free fall, but as time increases, the

curve gradually transforms from a curved state to an approximate straight line, with a slope equal to the ultimate velocity v_∞.

2.5. Polynomial Resistance Model

In more complex cases, multiple resistance effects, namely $F_d = av + bv^2 + cv^3 + \cdots$, can be considered comprehensively. Substituting into equation (1) yields:

$$m\frac{dv}{dt} = mg - (av + bv^2 + cv^3 + \cdots) \tag{14}$$

In the polynomial resistance model, it is difficult to obtain an explicit analytical solution for the evolution of an object's velocity over time, but its characteristics can still be analyzed through equilibrium conditions and numerical simulations. From the equilibrium equation $mg = av_\infty + bv_\infty{}^2 + cv_\infty{}^3 + \cdots$ of the ultimate velocity, it can be seen that the final velocity is determined by the combined effect of polynomial terms. In the low-speed range, linear terms dominate, and the motion process is close to a linear resistance model; In the medium to high speed section, the influence of the quadratic term gradually becomes apparent, and the curve characteristics are closer to the quadratic resistance model; In the case of ultra-high speed, higher-order terms such as cv^3 or even higher order terms may also make significant contributions, making the convergence process of speed faster.

3. Numerical Simulation and Result Analysis

In the previous section, theoretical deductions were made for different air resistance models, and analytical expressions for the variation of velocity and displacement over time were obtained. But in more complex situations, analytical solutions are difficult to obtain, and formulas alone are not sufficient to intuitively reflect the process of an object falling. Therefore, this article further adopts numerical simulation methods to calculate and visualize the motion laws of various models.

The simulation part is implemented based on Python programming language, using the fourth-order Runge Kutta (RK4) method to numerically integrate the motion differential equation, and combining with the trapezoidal integration method to calculate the displacement variation over time. By drawing speed time curves and displacement time curves, not only can the dynamic characteristics of objects under different resistance models be visually displayed, but the numerical results can also be compared with theoretical analytical solutions to verify the correctness of the derivation and analyze the differences between different models.

3.1. Constant Resistance Model Simulation and Analysis

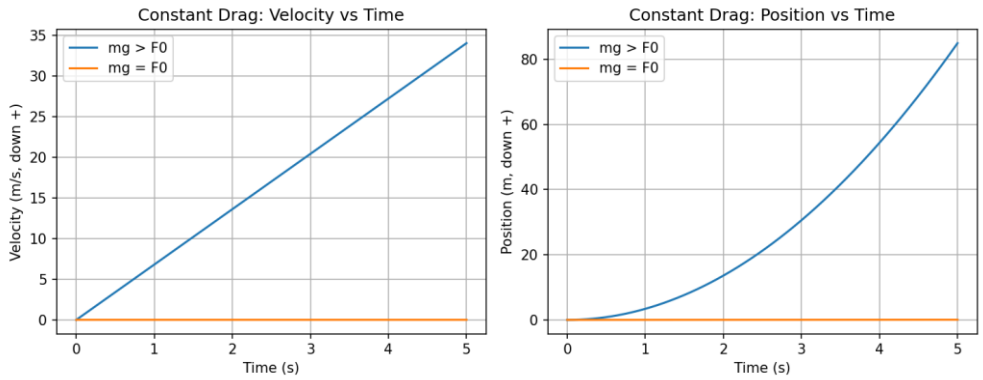

(a) Speed time variation chart (b) Displacement time variation chart

Figure 1. Schematic diagram of the variation of object velocity and displacement with time in the constant resistance model

In simulation, the mass $\mathrm{m} = 1\mathrm{kg}$ and gravitational acceleration $\mathrm{g} = 9.8\mathrm{m/s^2}$ are taken. When $F_0 = 3N$, $\mathrm{mg} > \mathrm{F_0}$ is satisfied; when $F_0 = 9.8N$, $\mathrm{mg} = \mathrm{F_0}$ is satisfied. The velocity and position curve data in Figure 1 were generated through Python simulation based on Equations (4) and (5), respectively.

In the constant resistance model, the magnitude of the air resistance experienced by an object is fixed at F_0 and is independent of velocity. The simulation results in Figure 1 (a) show that when $\mathrm{mg} > \mathrm{F_0}$ is reached, the velocity of the object increases linearly with time, and the velocity time curve takes the form of a straight line, indicating that its acceleration is a constant $\mathrm{a} = \mathrm{g} - \frac{\mathrm{F_0}}{\mathrm{m}}$. The curve in Figure 1 (b) is parabolic, which conforms to the law of constant acceleration motion. This indicates that in this model, air resistance only plays a role in weakening gravity, but is not enough to form a maximum velocity, and the object will still accelerate infinitely and fall. When $\mathrm{mg} = \mathrm{F_0}$ is used, the net force is zero, and the simulation results show that the object remains stationary, with both velocity and displacement curves being horizontal lines. Compared with linear and quadratic resistance models, the constant resistance model cannot reflect the characteristic of real air resistance increasing with velocity, and its applicability is limited. However, as a simplified model, it can intuitively demonstrate the weakening effect of resistance on acceleration, which has certain enlightening and comparative significance.

3.2. Linear Resistance Model Simulation and Analysis

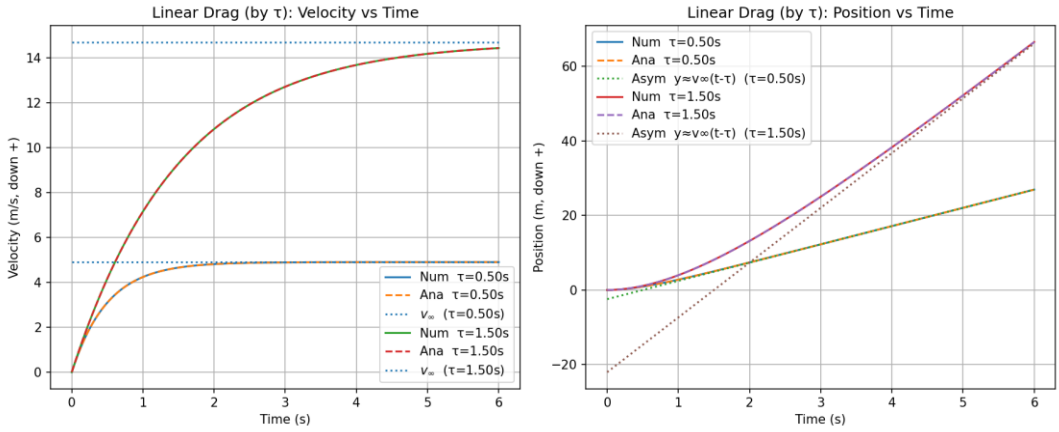

(a) Speed time variation chart (b) Displacement time variation chart

Figure 2. Schematic diagram of the variation of object velocity and displacement with time in the linear resistance model

In the simulation, the mass $\mathrm{m} = 1\mathrm{kg}$ and gravitational acceleration $\mathrm{g} = 9.8\mathrm{m/s^2}$ are taken. In order to compare different time scales, time constants $\tau = 0.5\mathrm{s}$ and $\tau = 01.5\mathrm{s}$ are set, and the corresponding drag coefficients are $\mathrm{k} = 2$ and $\mathrm{k} = \frac{2}{3}$, respectively. At this time, the maximum speeds are $v_\infty = 4.9m/s$ and $v_\infty = 14.7m/s$. Both the numerical and analytical solution data in Figure 2 were obtained through Python programming. The analytical solutions for velocity and displacement were simulated based on Equations (8) and (9), respectively, while the numerical solutions were calculated using the forward Euler integration method. Figure 2 shows the velocity time and displacement time curves under the linear resistance model, comparing the numerical solution (solid line) with the analytical solution (dashed line). The limit velocity horizontal line is added to the velocity graph, and the corresponding asymptotic line is added to the displacement graph. It can be seen that the numerical solution almost completely overlaps with the analytical solution, which verifies the accuracy of the numerical method.

In Figure 2 (a), the curves with different time constants show significant differences. When larger, the maximum speed v_∞ of the curve is higher, but it takes longer to approach steady state; When the limit speed is low, but the speed curve quickly approaches the horizontal line. The horizontal dashed

line visually indicates the maximum speed under different conditions, making the convergence trend of the curve clearer.

In Figure 2 (b), the initial curves are approximately parabolic, indicating that the influence of air resistance is weak during this stage, and the fall is close to free fall. As time increases, the curve gradually transforms into an approximate straight line, and its slope is the corresponding limit velocity. The added asymptotic straight line $y = v_\infty(t - \tau)$ remains parallel to the numerical curve over a long period of time, further verifying the conclusion in theoretical analysis that the slope of displacement in the later stage is equal to the ultimate velocity. At the same time, it can be observed that there is a significant difference in the slope of different corresponding lines, reflecting the determining effect of resistance strength on the displacement growth rate.

3.3. Simulation and Analysis of Secondary Resistance Model

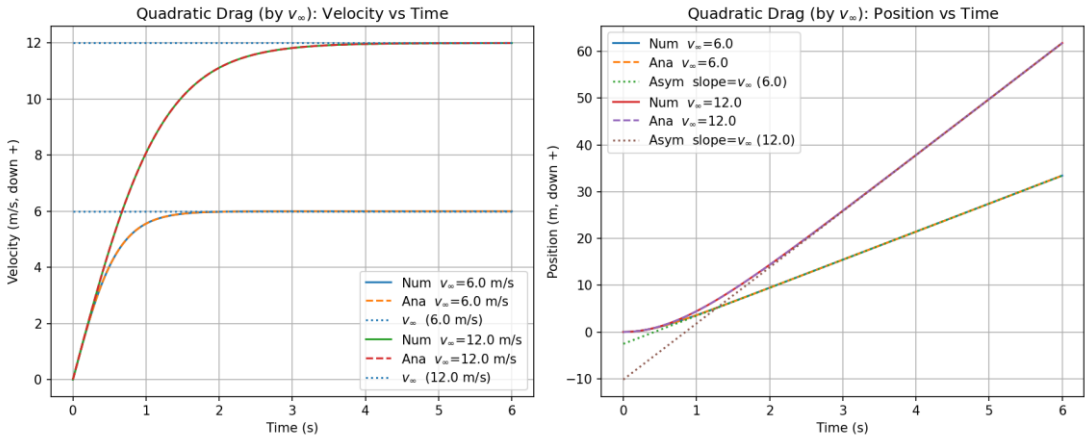

(a) Speed time variation chart (b) Displacement time variation chart

Figure 3. Schematic diagram of the variation of object velocity and displacement with time in the secondary resistance model

In the simulation, take the mass $m = 1kg$ and the gravitational acceleration $g = 9.8m/s^2$. Set the limit velocities $v_\infty = 6m/s$ and $v_\infty = 12m/s$ respectively. The corresponding resistance coefficients calculated are $c \approx 0.272$ and $c \approx 0.068$, respectively. In Figure 3, both the analytical and numerical solutions were implemented using Python. The analytical velocity and displacement curves were generated based on Equations (12) and (13), respectively, and the numerical solutions were obtained via the forward Euler method. Figure 3 shows the velocity time and displacement time curves under the quadratic resistance model, comparing the numerical solution (solid line) with the analytical solution (dashed line). The limit velocity reference line is added to the velocity graph, and the corresponding asymptotic line is added to the displacement graph. It can be seen that the numerical solution and analytical solution almost completely overlap throughout the entire time interval.

In Figure 3 (a), the curve quickly converges to the ultimate velocity of $v_\infty = \sqrt{\frac{mg}{c}}$ in the form of a hyperbolic tangent function. Different drag coefficients correspond to different ultimate velocities. When the drag is weak, v_∞ is larger, and the velocity curve tends to stabilize at higher positions, but the convergence process is relatively slow; When the resistance is strong, v_∞ is small, and the velocity curve converges at a lower horizontal line, but the convergence process is faster. The horizontal dashed line visually indicates the position of the maximum speed, making the asymptotic trend of speed over time clearer.

In Figure 3 (b), the initial stage curve is close to a parabola, indicating that the air resistance is not significant yet, and the object is falling close to free fall; As time goes by, the curve gradually transitions to an approximate straight line, and the slope is the ultimate speed. The added asymptotic straight line $y = v_\infty t - \frac{m}{c}\ln 2$ remains parallel to the numerical curve over a long period of time,

verifying the conclusion in theoretical analysis that 'displacement increases with the slope of the ultimate velocity in the later stage'. The difference in the slope of the asymptotic line under different resistance strengths reflects the influence of the magnitude of the ultimate velocity, thus reflecting the dominant role of air resistance in the high-speed range of the motion process.

3.4. Simulation and Analysis of Multiple Resistance Models

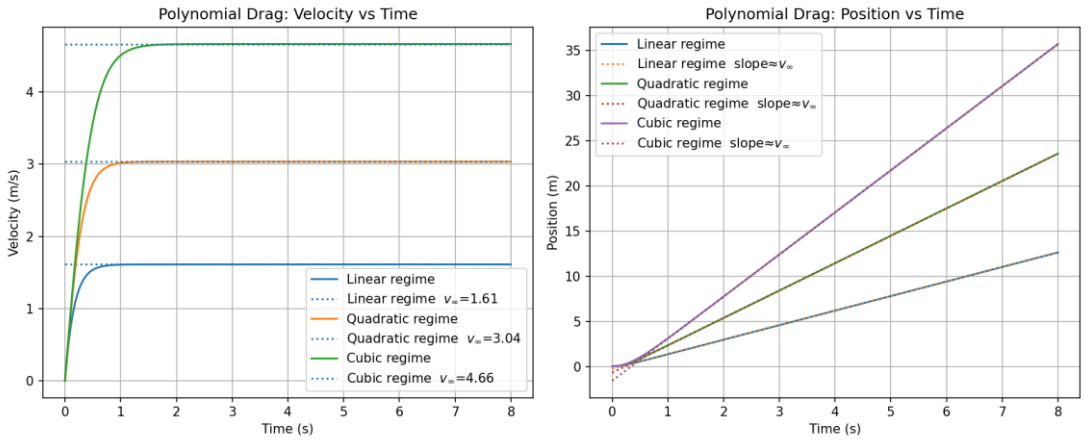

(a) Speed time variation chart (b) Displacement time variation chart

Figure 4. Schematic diagram of the variation of object velocity and displacement with time in the multi term resistance model

Figure 4 shows the velocity time and displacement time curves under the polynomial resistance model, considering three typical cases, Linear regime $a = 6.0, b = 0.05, c = 0$、Quadratic regime $a = 0.8, b = 0.80, c = 0$、Cubic regime $a = 0.5, b = 0.25, c = 0.02$. The solid lines in Figure 4 represent the numerical solutions obtained by integration using the forward Euler method. The dashed line in Figure 4(a) indicates the terminal velocity, while the straight line in Figure 4(b) represents an asymptotic line whose slope equals the terminal velocity in the later stage of motion.

In Figure 4 (a), it can be seen that all three scenarios converge to the ultimate velocity, but there is a significant difference between the convergence rate and the steady value. Under linear regime, the speed curve rises slowly and the maximum speed is relatively high; Under the Quadratic regime, due to the rapid increase of resistance with the square of velocity, the maximum velocity decreases significantly, and the velocity curve approaches the horizontal line faster; In the cubic regime, the introduction of the cubic term further enhances the resistance in the high-speed zone, causing the maximum speed to be further lowered and reaching steady state faster. The horizontal reference lines indicate their respective maximum speeds, making the convergence trend of the curve more intuitive.

In Figure 4 (b), the initial three curves are approximately parabolic, indicating that the drag effect is not significant during the low-speed stage, and the falling motion is close to free fall. As time increases, the curve gradually transforms into a straight line, and the slope corresponds exactly to the maximum speed in different situations. The added asymptotic line confirms this point: regardless of which resistance dominates, the displacement curve remains parallel to the reference line over a long period of time. It can be clearly observed that the slope of the linear region is the highest, indicating the fastest descent, followed by the quadratic region, while the slope of the cubic region is the lowest, indicating the slowest descent.

In summary, the polynomial resistance model not only unifies the motion laws in different speed ranges, but also demonstrates the segmented dominant role of resistance increasing with the power of velocity in the motion process. The low-speed stage is dominated by linear terms, the medium speed stage is dominated by quadratic terms, and the high-speed stage may require consideration of third-order and higher-order resistance terms. This model clearly reproduces the partition

characteristics in theoretical analysis through numerical simulation, providing a powerful tool for research in complex air resistance scenarios.

4. Conclusions

This article analyzes four types of air resistance models: constant, linear, quadratic, and polynomial, from both theoretical derivation and numerical simulation perspectives. The results indicate that different forms of resistance determine whether there is a limit value for object velocity and the speed at which it tends to steady state: constant resistance only weakens acceleration, linear resistance reflects exponential convergence under viscous flow, quadratic resistance quickly forms the limit velocity, and polynomial resistance uniformly demonstrates the segmented dominant effect in different velocity ranges. The simulation results are highly consistent with the theory, and the visualization of the limit velocity and asymptotic line makes the physical laws more intuitive. In the future, factors such as height and density can be further introduced on this basis to expand to more complex aerodynamic scenarios.

References

[1] Ong C R, Miura H, Koike M. The Terminal Velocity of Axisymmetric Cloud Drops and Raindrops Evaluated by the Immersed Boundary Method[J]. Journal of the Atmospheric Sciences, 2021, 78(4): 1129–1146.

[2] Zhang Z, Peng Z, Li X, Ma Z, Zhou P, Huang X. Shuttlecock trajectory during spin serves[J]. Physics of Fluids, 2025, 37(8): 087179.

[3] Zhou L. Aerodynamic characteristics and trajectory analysis of badminton shuttlecocks[J]. Acta of Bioengineering and Biomechanics, 2024, 26(4): 29–37.

[4] Uyanna O, Najafi H, Rajendra B. An inverse method for real-time estimation of aerothermal heating for thermal protection systems of space vehicles[J]. International Journal of Heat and Mass Transfer, 2021, 175: 121482.

[5] Chudinov P S. Projectile Motion in Midair Using Simple Analytical Approximations[J]. The Physics Teacher, 2022, 60(9): 774–778.

[6] Said A, Mshewa M, Mwakipunda G, Ngata M, Mohamed E. Computational Solution to the Problems of Projectile Motion under Significant Linear Drag Effect[J]. Open Journal of Applied Sciences, 2023, 13(4): 508–528.

[7] Bradshaw J L. Projectile motion with quadratic drag[J]. American Journal of Physics, 2023, 91(4): 258–263.

[8] Lubarda M V, Lubarda V A. A review of the analysis of wind-influenced projectile motion in the presence of linear and nonlinear drag force[J]. Archive of Applied Mechanics, 2022, 92(7): 1997–2017.

[9] Narkiewicz-Jodko R, Dominik A, Kozioł P. Subtle features in projectile motion with quadratic drag found through Taylor series expansions[J]. American Journal of Physics, 2022, 90(2): 135–141.

[10] Veeresha P, Thasi K, Khader M M. Computational analysis of the fluid–structure interactions of a synthetic badminton shuttlecock at various flight speeds[J]. Physics of Fluids, 2024, 36(1): 015113.